Signal Processing 157 (2019) 119–130

Contents lists available at ScienceDirect

Signal Processing

journal homepage: www.elsevier.com/locate/sigpro

Passive localization and classification of mixed near-field and far-field sources based on high-order differencing algorithm

Amir Masoud Molaei, Bijan Zakeri*, Seyed Mehdi Hosseini Andargoli

Electrical and Computer Engineering Department, Babol Noshirvani University of Technology, Babol, Iran

ARTICLE INFO

Article history:
Received 17 July 2018
Revised 24 November 2018
Accepted 26 November 2018
Available online 27 November 2018

Keywords:
High-order differencing
Proper number of snapshots
Multiple mixed near-field and far-field sources

ABSTRACT

A novel method called high-order differencing algorithm (HODA) is presented for localization of mixed sources. Five special cumulant matrices are constructed. The first one only contains the angle information. By modifying its rank and using an ESPRIT-like approach, the initial DOA set (IDOAS) is formed. The four others, pairwise, contain common far-field information. By two differencing operations, the far-field information is eliminated, and the difference cumulant matrices (DCMs) are obtained. After the rank modification is executed, the DCMs are reconstructed. By applying an ESPRIT-like approach to them, electrical angles are extracted. The extracted data is compared with IDOAS to obtain valid information of near-field sources (NFSs). A mechanism called kurtosis testing algorithm (KTA) is presented for identifying far-field sources (FFSs). KTA is able to identify even those FFSs that are located at the same angle with NFSs. To control the error of statistical differencing, an appropriate number of snapshots is considered. Analyses show that HODA prevents aperture loss; it does not require pairing, knowing the number of NFSs or FFSs, and heavy searches. The results confirm its good performance in terms of classification, the correct estimation of sources with different fields and the same DOAs, estimation accuracy and computational complexity.

1. Introduction

The passive radio systems do not emit any signal. They can work as a complement to active ones. Their development requires strong processors and some new technologies. When sources are located in the near-field (NF) region of the array, the received signals are a non-linear function of the DOA, which results in the high complexity of the localization. In the case of near-field source (NFS), in addition to estimating both the DOA and range, the pairing between these two must also be made. In some practical applications, such as electronic supervision, guidance systems, seismic exploration, and speaker localization, any source can be located at far-field (FF) or NF. Since traditional methods inherently require just FF or NF signals, in recent years, there has been growing attention in the issue of mixed sources localization.

The mixed NFSs and far-field sources (FFSs) localization was first presented by an efficient two-stage MUSIC (TSMUSIC) algorithm [1], using fourth-order cumulant (FOC) and spectral search. An algorithm called oblique projection MUSIC (OPMUSIC) is presented in [2], which only uses second-order statistics (SOS). Xie et al. in [3] provide a MUSIC-MVDR based approach that uses spatial-temporal fourth-order statistics (FOS) and does not need to know the number of sources. The covariance differencing method presented in [4,5], entitled two-stage matrix differencing algorithm (TSMDA), provides a more reasonable classification of the signals types.

All of the above methods require heavy spectral search computations. Meanwhile, TSMUSIC and method of [3] have more processing volume due to the utilization of both FOS and heavy spectral search. The relatively severe loss of the aperture which is observed in OPMUSIC and TSMDA is another problem which should be considered. The use of high-order statistics (HOS), in addition to increasing the estimation accuracy, also it saves the number of sensors [6]. Furthermore, the FOC is not sensitive to any kind of Gaussian noise. The differencing presented in TSMDA is valid only for SOS. According to what we will show in the text, for the FOS, the Toeplitz property used in [4,5] will no longer help to separate the NF and FF components. What will be presented in this paper is a novel method called high-order differencing algorithm (HODA), which in addition to the effective separation of the FF and NF components in the FOS domain, it allows the localization of the NFSs and FFSs without any heavy spectral search, pairing process, and severe aperture loss.

HODA receives data through a symmetric uniform linear array (ULA). First, the proper number of snapshots is determined and

* Corresponding author.
E-mail address: zakeri@nit.ac.ir (B. Zakeri).

https://doi.org/10.1016/j.sigpro.2018.11.018
0165-1684/

then five special cumulant matrices are constructed. The first one of them contains the angle information only. By modifying its rank and using an ESPRIT-like approach, the angles are extracted and the initial DOA set (IDOAS) is formed. The four others, pairwise, contain common FF information. By two simple differencing operations, the information of FFSs is eliminated, and the difference cumulant matrices (DCMs) are obtained. After modifying their rank, the DCMs are reconstructed. By applying an ESPRIT-like approach, electrical angles are extracted and the extracted data is compared with IDOAS to obtain valid DOAs of NFSs and their ranges. Also, a mechanism called kurtosis testing algorithm (KTA) is presented for identifying FFSs.

The rest of this paper is organized as follows: in Section 2, data model and main assumptions are expressed; in Section 3, the proposed algorithm is fully explained; in Section 4, discussions are presented; Section 5 is devoted to simulations and their results; conclusions are presented in Section 6.

2. Data model

Assume K uncorrelated narrowband sources including K_N NFSs and K_F FFSs. The signals transmitted by these sources, from directions $\theta_1, \theta_2, ..., \theta_K$ impinge on a symmetric ULA of $N = 2M + 1$ elements whose inter-spacing being d. Each element is denoted by index l, where $l = -M, ..., 0, ..., M$. For lth sensor and the ith signal, the array steering vector a_{li} is defined by $e^{jT_{li}}$, where $i = 1, 2, ..., K$. Considering the array center as the phase reference, the phase shift T_{li} is of the form [7]

$$T_{li} = 2\pi r_i \left(\sqrt{1 + (ld/r_i)^2 - 2ld \sin\theta_i / r_i} - 1 \right) / \lambda \tag{1}$$

where λ is the wavelength, and r_i is the range of ith source. In the Fresnel region, which is defined as $[0.62(D^3/\lambda)^{1/2}, 2D^2/\lambda]$ where D symbolizes the array aperture, a simplification of the model in Eq. (1) is used as a good approximation and given by [7]

$$T_{li} \approx \gamma_i l + \phi_i l^2, \quad For\ NFS \tag{2}$$

where the electric angles γ_i and ϕ_i are obtained by [8]

$$\gamma_i = -2\pi d \sin\theta_i / \lambda \quad and \quad \phi_i = \pi d^2 \cos^2\theta_i / \lambda r_i. \tag{3}$$

For the FFS, the range parameter is assumed to be ∞ and the associated term ϕ_i is approximated by zero. In other words, we have

$$T_{li} \approx \gamma_i l, \quad For\ FFS. \tag{4}$$

Without the loss of generality, assume the first K_N signals are received from the NF and the others from the FF. After sampled with a proper sampling rate, and with Eqs. (2)–(4), the tth sample of the signal observed by the lth sensor can be expressed as [8]

$$x_l(t) = \sum_{i=1}^{K_N} s_i(t)\, e^{j(\gamma_i l + \phi_i l^2)} + \sum_{i=K_N+1}^{K} s_i(t)\, e^{j\gamma_i l} + n_l(t) \tag{5}$$

where $t = 1, ..., L$. L, $s_i(t)$ and $n_l(t)$ are the snapshot number, baseband signal of the ith source, and noise of the lth sensor. In a matrix form, the array output can be expressed as

$$\mathbf{x}(t) = \mathbf{A}\,\mathbf{s}(t) + \mathbf{n}(t) \tag{6}$$

where

$$\begin{aligned} &\mathbf{x}(t) = [x_{-M}(t) \cdots x_0(t) \cdots x_M(t)]^T, \quad \mathbf{s}(t) = \left[\mathbf{s}_N^T(t)\, \mathbf{s}_F^T(t)\right]^T, \\ &\mathbf{s}_N(t) = [s_1(t) \cdots s_{K_N}(t)]^T, \quad \mathbf{s}_F(t) = [s_{K_N+1}(t) \cdots s_K(t)]^T, \\ &\mathbf{n}(t) = [n_{-M}(t) \cdots n_0(t) \cdots n_M(t)]^T \end{aligned} \tag{7}$$

where $\mathbf{s}_N(t) \in \mathbb{C}^{K_N \times 1}$ and $\mathbf{s}_F(t) \in \mathbb{C}^{K_F \times 1}$ signifies the source vector of the NF and FF signals, respectively. $\mathbf{n}(t) \in \mathbb{C}^{N \times 1}$ is the additive Gaussian noise vector with mean zero. $\mathbf{A} \in \mathbb{C}^{N \times K}$ symbolizes the steering matrix and can be written as

$$\begin{aligned} &\mathbf{A} = [\mathbf{A}_N\, \mathbf{A}_F], \quad \mathbf{A}_N = [\mathbf{a}_1\, \mathbf{a}_2 \cdots \mathbf{a}_{K_N}], \quad \mathbf{A}_F = [\mathbf{a}_{K_N+1}\, \mathbf{a}_{K_N+2} \cdots \mathbf{a}_K], \\ &\mathbf{a}_i = [a_{-Mi}\, a_{-M+1i} \cdots a_{Mi}]^T. \end{aligned} \tag{8}$$

Throughout the paper, the following assumptions are made:

[A1] The signals are mutually independent, narrowband stationary processes, non-Gaussian and with nonzero kurtosis.
[A2] The noise is the additive (white or color) Gaussian one, and statistically independent of the signals.
[A3] The sensor array is a ULA which is arranged by element spacing $d \le \lambda/4$, in order to avoid the phase ambiguity [9].
[A4] DOAs are not the same for FFSs; DOAs of NFSs are also different, but the FFS can be located at the same angle with the NFS.

3. Proposed algorithm

3.1. Definitions

We define five special cross-cumulant for the array output signals with common time lag 0 and different sensor lags in the following form:

$$\begin{aligned} c_{x,1} &= Cum_4\left\{x_{u+1}^*(t), x_{u+2}(t), x_{v+2}^*(t), x_{v+1}(t)\right\} \\ c_{x,2} &= Cum_4\left\{x_{u+1}^*(t), x_{u+2}(t), x_{v+1}^*(t), x_v(t)\right\} \\ c_{x,3} &= Cum_4\left\{x_u^*(t), x_{u+1}(t), x_{M-v}^*(t), x_{M+1-v}(t)\right\} \\ c_{4x,4} &= Cum_4\left\{x_{u+1}^*(t), x_{u+2}(t), x_{M-v}^*(t), x_{M+1-v}(t)\right\} \\ c_{x,5} &= Cum_4\left\{x_{-\bar{v}}^*(t), x_{-\bar{u}}(t), x_{\bar{u}}^*(t), x_{\bar{v}}(t)\right\} \end{aligned} \tag{9}$$

where $u, v \in [-M, M-2]$ and $\bar{u}, \bar{v} \in [-M, M]$. For example, the first cumulant is calculated as follows:

$$\begin{aligned} c_{x,1} = {} & E\left\{x_{u+1}^*(t) x_{u+2}(t) x_{v+2}^*(t) x_{v+1}(t)\right\} \\ & - E\left\{x_{u+1}^*(t) x_{u+2}(t)\right\} E\left\{x_{v+2}^*(t) x_{v+1}(t)\right\} \\ & - E\left\{x_{u+1}^*(t) x_{v+2}^*(t)\right\} E\{x_{u+2}(t) x_{v+1}(t)\} \\ & - E\left\{x_{u+1}^*(t) x_{v+1}(t)\right\} E\left\{x_{u+2}(t) x_{v+2}^*(t)\right\}. \end{aligned} \tag{10}$$

Other cumulants can also be expressed in a similar manner. According to [A1], [A2] and Eq. (10), the results of the cumulants of Eq. (9) can be written as

$$\begin{aligned} c_{x,1} \ (=) & \sum_{i=1}^{K_N} c_i e^{j2\phi_i(u-v)} + \sum_{i=K_N+1}^{K} c_i, \quad c_{x,2} = \sum_{i=1}^{K_N} c_i e^{j2\phi_i(u-v)}\, e^{j2\phi_i} + \sum_{i=K_N+1}^{K} c_i, \\ c_{x,3} = {} & \sum_{i=1}^{K_N} c_i e^{j2\phi_i(u-v)}\, e^{j2\gamma_i} + \sum_{i=K_N+1}^{K} c_i e^{j2\gamma_i}, \\ c_{x,4} = {} & \sum_{i=1}^{K_N} c_i e^{j2\phi_i(u-v)}\, e^{j2\gamma_i}\, e^{j2\phi_i} + \sum_{i=K_N+1}^{K} c_i e^{j2\gamma_i}, \\ c_{x,5} = {} & \sum_{i=1}^{K} c_i e^{-j2(\bar{u}-\bar{v})\gamma_i} \end{aligned} \tag{11}$$

where $c_i = Cum_4\{s_i^*(t), s_i(t), s_i^*(t), s_i(t)\}$ is the kurtosis related to the ith signal with the time lag 0. According to Eq. (11), and by collecting all the sensor lags (for all values u, v, $\bar{u}$ and $\bar{v}$), we can construct the complex cross-cumulant matrices in the following form:

$$\begin{aligned} &\mathbf{C}_1 = \mathbf{B}\mathbf{C}_s\mathbf{B}^H, \quad \mathbf{C}_2 = \mathbf{B}\mathbf{C}_s\mathbf{\Phi}\mathbf{B}^H, \quad \mathbf{C}_3 = \mathbf{B}\mathbf{C}_s\mathbf{Y}\mathbf{B}^H, \\ &\mathbf{C}_4 = \mathbf{B}\mathbf{C}_s\mathbf{\Phi}\mathbf{Y}\mathbf{B}^H, \quad \mathbf{C}_5 = \mathbf{E}\mathbf{C}_s\mathbf{E}^H. \end{aligned} \tag{12}$$

where $\mathbf{C}_s = diag[c_1, ..., c_K] \in \mathbb{R}^{K \times K}$, $\mathbf{Y} = diag[e^{j2\gamma_1}, ..., e^{j2\gamma_K}] \in \mathbb{C}^{K \times K}$ and $\mathbf{\Phi} = diag[e^{j2\phi_1}, ..., e^{j2\phi_{K_N}}, 1, ..., 1] \in \mathbb{C}^{K \times K}$. $\mathbf{B} \in \mathbb{C}^{(N-2) \times K}$ is a

matrix of rank K_N+1 (according to [A4]), whose elements of the last K_F columns are equal to 1, and elements of the first K_N columns contain information of electric angles ϕ_i. It is obtained by

$$\mathbf{B}=\begin{bmatrix} e^{-j2M\phi_1} & e^{-j2M\phi_2} & \cdots & e^{-j2M\phi_{K_N}} & 1 & \cdots & 1 \\ e^{j2(-M+1)\phi_1} & e^{j2(-M+1)\phi_2} & \cdots & e^{j2(-M+1)\phi_{K_N}} & 1 & \cdots & 1 \\ \vdots & \vdots & \ddots & \vdots & \vdots & \ddots & \vdots \\ e^{j2(M-2)\phi_1} & e^{j2(M-2)\phi_2} & \cdots & e^{j2(M-2)\phi_{K_N}} & 1 & \cdots & 1 \end{bmatrix}. \tag{13}$$

Also, $\mathbf{E}\in\mathbb{C}^{N\times K}$ is obtained by

$$\mathbf{E}=\begin{bmatrix} e^{j(N-1)\gamma_1} & e^{j(N-1)\gamma_2} & \cdots & e^{j(N-1)\gamma_K} \\ e^{j(N-3)\gamma_1} & e^{j(N-3)\gamma_2} & \cdots & e^{j(N-3)\gamma_K} \\ \vdots & \vdots & \ddots & \vdots \\ e^{-j(N-1)\gamma_1} & e^{-j(N-1)\gamma_2} & \cdots & e^{-j(N-1)\gamma_K} \end{bmatrix}. \tag{14}$$

3.2. Proper selection of snapshot number

Remaining effects of other components in the differencing of statistical matrices with a finite number of snapshots is unavoidable. To reduce the estimation errors caused by such a process, here we introduce a pre-processing for the proper selection of snapshot number.

Different sensor lags make different phases in the received signal. So, if we only use data that, as far as possible, includes the full cycles of all signals, the errors can be reduced. Given the unknown frequency of signals, we need to first estimate the frequency of the baseband signals having L snapshots. Suppose f_i is the linear frequency of the ith signal. By extracting the pseudospectrum using the MUSIC approach [10,11], we can estimate the f_is where $i=1,\ ...,\ K$. The appropriate number of snapshots for use in HODA is obtained from the following equation:

$$L_P = L - rem\left(L,\ f_s\times LCM\left(\left[1/\hat{f}_1\right],\ ...,\ \left[1/\hat{f}_K\right]\right)\right) \tag{15}$$

where f_s is the sampling frequency in Hz, and $rem(a,b)$ returns the remainder after the division of a by b. All statistical matrices defined in Section 3.1 are estimated based on L_p snapshots.

3.3. Sources DOA estimation

In HODA, information of the first four matrices constructed in Eq. (12) is not sufficient to find the DOA of FFSs and the number of NFSs. The fifth matrix only contains the DOAs information. Here, we will reconstruct $\mathbf{C}_5$ in a way so that its rank becomes equal to the known value of K. Assuming that $\Upsilon_5=[\upsilon_{5,1},\ ...,\ \upsilon_{5,N}]\in\mathbb{C}^{N\times N}$ and $\varsigma_5=[\mathbf{v}_{5,1},\ ...,\ \mathbf{v}_{5,N}]\in\mathbb{C}^{N\times N}$ are the left and right singular vectors of $\mathbf{C}_5$, respectively, and that $\mathbf{\Sigma}_5=diag[\sigma_{5,1},\ ...,\ \sigma_{5,N}]\in\mathbb{R}^{N\times N}$ indicates the singular values of $\mathbf{C}_5$ (where $\sigma_{5,1}\geq\cdots\geq\sigma_{5,N}$), we form the reconstructed Hermitian matrix $\breve{\mathbf{C}}_5$ as

$$\breve{\mathbf{C}}_5=\Upsilon'_5\mathbf{\Sigma}'_5\varsigma'^{H}_5 \tag{16}$$

where $\Upsilon'_5=[\upsilon_{5,1},\ ...,\ \upsilon_{5,K}]\in\mathbb{C}^{N\times K}$, $\varsigma'_5=[\mathbf{v}_{5,1},\ ...,\ \mathbf{v}_{5,K}]\in\mathbb{C}^{N\times K}$ and $\mathbf{\Sigma}'_5=diag\,[\sigma_{5,1},\ ...,\ \sigma_{5,K}]\in\mathbb{R}^{K\times K}$. $\breve{\mathbf{C}}_5$ can be divided into two overlapping matrices $\breve{\mathbf{C}}_{51}\in\mathbb{C}^{2M\times N}$ and $\breve{\mathbf{C}}_{52}\in\mathbb{C}^{2M\times N}$, which are comprised of the first and last $2M$ rows of $\breve{\mathbf{C}}_5$, respectively. Considering [A4] and that $N\geq K$, $\mathbf{E}^H$ is full row rank. Therefore, we form the *DOA estimation matrix* as

$$\mathbf{C}_{DOA}=\breve{\mathbf{C}}_{51}^{\dagger}\breve{\mathbf{C}}_{52}. \tag{17}$$

By applying the eigenvalue decomposition (EVD) to $\mathbf{C}_{DOA}$, we have

$$\mathbf{C}_{DOA}=\Upsilon\mathbf{\Sigma}\Upsilon^{-1} \tag{18}$$

where $\mathbf{\Sigma}=diag[\rho_1,\ ...,\ \rho_N]$ is the eigenvalues vector with the elements arranged as $|\rho_1|\geq\cdots\geq|\rho_K|>|\rho_{K+1}|\geq\cdots\geq|\rho_N|$. A part of $\Upsilon\in\mathbb{C}^{N\times N}$ is composed of K eigenvectors related to $\rho_1,...,\rho_K$, which span the signal subspace of $\mathbf{C}_{DOA}$. Therefore, it would be easy to estimate the DOAs as

$$\hat{\theta}_i=\arcsin\left(\lambda\angle\rho_i/4\pi d\right),\quad i=1,\ ...,\ K \tag{19}$$

where $\rho_i=e^{-j2\hat{\gamma}_i}$. The *initial DOA set (IDOAS)* can be considered as $\hat{\theta}=\{\hat{\theta}_1,\ ...,\ \hat{\theta}_{K_N},\ \hat{\theta}_{K_N+1},\ ...,\ \hat{\theta}_K\}$. However, Eq. (19) alone cannot determine which DOAs belong to the NF and FF sources.

3.4. Separation of NF and FF components

With regard to the definitions in Section 3.1, we now show how to separate the NF and FF components by differencing in the FOS domain. Each of the first four cumulant matrices in Eq. (12) can be written as a sum of two cumulant matrices; one containing only the NF components, and the other one containing only the FF information, namely

$$\mathbf{C}_1=\mathbf{C}_{1N}+\mathbf{C}_{1F},\quad \mathbf{C}_2=\mathbf{C}_{2N}+\mathbf{C}_{1F},\quad \mathbf{C}_3=\mathbf{C}_{3N}+\mathbf{C}_{2F},\quad \mathbf{C}_4=\mathbf{C}_{4N}+\mathbf{C}_{2F} \tag{20}$$

where $\mathbf{C}_{1N}$, $\mathbf{C}_{2N}$, $\mathbf{C}_{3N}$, $\mathbf{C}_{4N}$, $\mathbf{C}_{1F}$ and $\mathbf{C}_{2F}$ are presented in Eq. (21), as shown at the bottom of next page. $\mathbf{J}_{N-2}$ is a unit matrix of the size $(N-2)\times(N-2)$. The matrices of Eq. (21) are all Toeplitz. Therefore, applying the technique of TSMDA is not applicable here for FOS. By two simple differencing between pairs of $\mathbf{C}_1$, $\mathbf{C}_2$, and $\mathbf{C}_3$, $\mathbf{C}_4$, we have

$$\mathbf{C}_{1N}=\begin{bmatrix} c_1+\cdots+c_{K_N} & c_1e^{-j2\phi_1}+\cdots+c_{K_N}e^{-j2\phi_{K_N}} & \cdots & c_1e^{-j2(N-3)\phi_1}+\cdots+c_{K_N}e^{-j2(N-3)\phi_{K_N}} \\ c_1e^{j2\phi_1}+\cdots+c_{K_N}e^{j2\phi_{K_N}} & c_1+\cdots+c_{K_N} & \cdots & c_1e^{-j2(N-4)\phi_1}+\cdots+c_{K_N}e^{-j2(N-4)\phi_{K_N}} \\ \vdots & \vdots & \ddots & \vdots \\ c_1e^{j2(N-3)\phi_1}+\cdots+c_{K_N}e^{j2(N-3)\phi_{K_N}} & c_1e^{j2(N-4)\phi_1}+\cdots+c_{K_N}e^{j2(N-4)\phi_{K_N}} & \cdots & c_1+\cdots+c_{K_N} \end{bmatrix},$$

$$\mathbf{C}_{2N}=\begin{bmatrix} c_1e^{j2\phi_1}+\cdots+c_{K_N}e^{j2\phi_{K_N}} & c_1+\cdots+c_{K_N} & \cdots & c_1e^{-j2(N-4)\phi_1}+\cdots+c_{K_N}e^{-j2(N-4)\phi_{K_N}} \\ c_1e^{j4\phi_1}+\cdots+c_{K_N}e^{j4\phi_{K_N}} & c_1e^{j2\phi_1}+\cdots+c_{K_N}e^{j2\phi_{K_N}} & \cdots & c_1e^{-j2(N-5)\phi_1}+\cdots+c_{K_N}e^{-j2(N-5)\phi_{K_N}} \\ \vdots & \vdots & \ddots & \vdots \\ c_1e^{j2(N-2)\phi_1}+\cdots+c_{K_N}e^{j2(N-2)\phi_{K_N}} & c_1e^{j2(N-3)\phi_1}+\cdots+c_{K_N}e^{j2(N-3)\phi_{K_N}} & \cdots & c_1e^{j2\phi_1}+\cdots+c_{K_N}e^{j2\phi_{K_N}} \end{bmatrix},$$

$$\mathbf{C}_{3N}=\begin{bmatrix} c_1e^{j2\gamma_1}+\cdots+c_{K_N}e^{j2\gamma_{K_N}} & c_1e^{-j2\phi_1}e^{j2\gamma_1}+\cdots & \cdots & c_1e^{-j2(N-3)\phi_1}e^{j2\gamma_1}+\cdots+c_{K_N}e^{-j2(N-3)\phi_{K_N}}e^{j2\gamma_{K_N}} \\ c_1e^{j2\phi_1}e^{j2\gamma_1}+\cdots+c_{K_N}e^{j2\phi_{K_N}}e^{j2\gamma_{K_N}} & c_1e^{j2\gamma_1}+\cdots & \cdots & c_1e^{-j2(N-4)\phi_1}e^{j2\gamma_1}+\cdots+c_{K_N}e^{-j2(N-4)\phi_{K_N}}e^{j2\gamma_{K_N}} \\ \vdots & \vdots & \ddots & \vdots \\ c_1e^{j2(N-3)\phi_1}e^{j2\gamma_1}+\cdots+c_{K_N}e^{j2(N-3)\phi_{K_N}}e^{j2\gamma_{K_N}} & c_1e^{j2(N-4)\phi_1}e^{j2\gamma_1}+\cdots & \cdots & c_1e^{j2\gamma_1}+\cdots+c_{K_N}e^{j2\gamma_{K_N}} \end{bmatrix},$$

$$\mathbf{C}_{4N}=\begin{bmatrix} c_1e^{j2\phi_1}e^{j2\gamma_1}+\cdots+c_{K_N}e^{j2\phi_{K_N}}e^{j2\gamma_{K_N}} & c_1e^{j2\gamma_1}+\cdots & \cdots & c_1e^{-j2(N-4)\phi_1}e^{j2\gamma_1}+\cdots+c_{K_N}e^{-j2(N-4)\phi_{K_N}}e^{j2\gamma_{K_N}} \\ c_1e^{j4\phi_1}e^{j2\gamma_1}+\cdots+c_{K_N}e^{j4\phi_{K_N}}e^{j2\gamma_{K_N}} & c_1e^{j2\phi_1}e^{j2\gamma_1}+\cdots & \cdots & c_1e^{-j2(N-5)\phi_1}e^{j2\gamma_1}+\cdots+c_{K_N}e^{-j2(N-5)\phi_{K_N}}e^{j2\gamma_{K_N}} \\ \vdots & \vdots & \ddots & \vdots \\ c_1e^{j2(N-4)\phi_1}e^{j2\gamma_1}+\cdots+c_{K_N}e^{j2(N-4)\phi_{K_N}}e^{j2\gamma_{K_N}} & c_1e^{j2(N-5)\phi_1}e^{j2\gamma_1}+\cdots & \cdots & c_1e^{j2\phi_1}e^{j2\gamma_1}+\cdots+c_{K_N}e^{j2\phi_{K_N}}e^{j2\gamma_{K_N}} \end{bmatrix},$$
$$\mathbf{C}_{1F}=(c_{K_N+1}+\cdots+c_K)\mathbf{J}_{N-2},\quad \mathbf{C}_{2F}=\left(c_{K_N+1}e^{j2\gamma_{K_N+1}}+\cdots+c_Ke^{j2\gamma_K}\right)\mathbf{J}_{N-2} \tag{21}$$

$$\mathbf{C}_{21}=\mathbf{C}_2-\mathbf{C}_1=\mathbf{C}_{2N}-\mathbf{C}_{1N},\quad \mathbf{C}_{43}=\mathbf{C}_4-\mathbf{C}_3=\mathbf{C}_{4N}-\mathbf{C}_{3N}. \tag{22}$$

The DCMs $\mathbf{C}_{21}, \mathbf{C}_{43}\in\mathbb{C}^{(N-2)\times(N-2)}$ contain only the NF components and are constructed utilizing Eqs. (12) and (22). In this way, we could separate the pure NF components from the entire data in the cumulant domain. Note that, the estimations will be based on the DCMs, that is, they will be dependent on the first K_N columns of $\mathbf{B}$, namely $\mathbf{B}_N$.

3.5. DOA identification and range estimation for NFSs

The DCMs in Eq. (22) can be decomposed into the multiplication of the matrices $\mathbf{B}_N$, $\mathbf{C}_{sN}$, $\mathbf{\Upsilon}_N$ and $\mathbf{\Phi}_N$, and rewritten as

$$\mathbf{C}_{21}=\mathbf{B}_N\mathbf{C}_{sN}\mathbf{\Phi}_N\mathbf{B}_N^H,\quad \mathbf{C}_{43}=\mathbf{B}_N\mathbf{C}_{sN}\mathbf{\Phi}_N\mathbf{\Upsilon}_N\mathbf{B}_N^H \tag{23}$$

where, the diagonal matrices $\mathbf{C}_{sN}$, $\mathbf{\Upsilon}_N$, $\mathbf{\Phi}_N\in\mathbb{C}^{K_N\times K_N}$ are obtained from the following:

$$\begin{aligned}&\mathbf{C}_{sN}=diag[c_1,\ ...,\ c_{K_N}],\quad \mathbf{\Upsilon}_N=diag\left[e^{j2\gamma_1},\ ...,\ e^{j2\gamma_{K_N}}\right],\\ &\mathbf{\Phi}_N=diag\left[j2e^{j\phi_1}\sin\phi_1,\ ...,\ j2e^{j\phi_{K_N}}\sin\phi_{K_N}\right]\end{aligned} \tag{24}$$

The columns of $\mathbf{B}_N\in\mathbb{C}^{(N-2)\times K_N}$ are composed of the first K_N columns of $\mathbf{B}$. With [A4], in order for $\mathbf{B}_N$ to be full column rank, it is necessary and sufficient that the number of sensors satisfy the condition $N\geq K_N+2$.

The two equations expressed in Eq. (23) can be considered as the basic equations of the ESPRIT [12]. If $\mathbf{B}_N$ is full column rank, then it can easily be shown that $\mathbf{B}_N^H$ is full row rank. In addition, according to [A1], $\mathbf{C}_{sN}$ has no zero singular value, and there are no two identical elements on the main diagonal of $\mathbf{\Upsilon}_N$ and $\mathbf{\Phi}_N$ (even for $\theta=\pm\pi/2$). We define the *NF estimation matrix* $\mathbf{C}_N\in\mathbb{C}^{(N-2)\times(N-2)}$ as

$$\mathbf{C}_N=\mathbf{C}_{21}\mathbf{C}_{43}^{\dagger}=\mathbf{B}_N\mathbf{C}_{sN}\mathbf{\Phi}_N\mathbf{B}_N^H\left(\mathbf{B}_N^H\right)^{\dagger}\mathbf{C}_{sN}^{-1}\mathbf{\Phi}_N^{-1}\mathbf{\Upsilon}_N^{-1}\mathbf{B}_N^{\dagger}=\mathbf{B}_N\mathbf{\Upsilon}_N^{-1}\mathbf{B}_N^{\dagger}. \tag{25}$$

The theoretical rank of $\mathbf{C}_N$ is equal to the number of NFSs that span the signal subspace and coincides with the range space of $\mathbf{B}_N$. In practice, because of the averaging of a finite number of snapshots, the correlation between the waves which are forming the matrices $\mathbf{C}_{21}$ and $\mathbf{C}_{43}$ is not completely zero. As a result, the rank of $\mathbf{C}_N$ is greater than K_N, in practice. Similar to the trick used in Section 3.3, we reconstruct $\mathbf{C}_{21}$ and $\mathbf{C}_{43}$ in a way so that their ranks become equal to the known value of K. Thus, the reconstructed matrix $\breve{\mathbf{C}}_N=\breve{\mathbf{C}}_{21}\breve{\mathbf{C}}_{43}^{\dagger}$ has K non-zero eigenvalues, and so, its rank is equal to K.

Given that $\mathbf{B}_N$ is full column rank, for estimating the electric angles of the NFSs we just need to apply an EVD to $\breve{\mathbf{C}}_N\in\mathbb{C}^{(N-2)\times(N-2)}$ as

$$\breve{\mathbf{C}}_N=\mathbf{H}\mathbf{\Lambda}\mathbf{H}^{-1} \tag{26}$$

where $\mathbf{\Lambda}=diag[\chi_1,\ ...,\ \chi_{N-2}]\in\mathbb{C}^{(N-2)\times(N-2)}$ has eigenvalues arranged as $|\chi_1|\geq\cdots\geq|\chi_K|>|\chi_{K+1}|=\cdots=|\chi_{N-2}|=0$. $\mathbf{H}\in\mathbb{C}^{(N-2)\times(N-2)}$ is the matrix of eigenvectors with column vectors $\mathbf{h}_m$, where $m=1,\ ...,\ N-2$. K_N eigenvalues (among from K non-zero eigenvalues) derived from the EVD of $\breve{\mathbf{C}}_N$, provide an estimate of the diagonal elements of $\mathbf{\Upsilon}_N^{-1}$ (i.e. $e^{-j2\hat{\gamma}_i}$, where $i=1,\ 2,\ ...,\ K_N$) containing the angular information of the NFSs. Therefore, we can select the azimuth angle of the NFSs from the estimated values of the following equation:

$$\hat{\vartheta}_i=\arcsin\left(\lambda\angle\mu_i/4\pi d\right),\quad i=1,\ ...,\ K. \tag{27}$$

K_N common values of $\hat{\vartheta}_i$ s and estimated DOAs in Eq. (19) are taken as the members of the *NFSs' azimuth angles vector* $\hat{\theta}_N\in\mathbb{R}^{1\times K_N}$, namely

$$\hat{\theta}_N=\left\{\hat{\theta}_i|\,\hat{\theta}_i\simeq\hat{\vartheta}_{i'},\ \ i,\,i'=1,\ 2,\ ...,\ K\right\}. \tag{28}$$

On the other hand, K_N eigenvectors $\mathbf{h}_m$ $(m=1,\ ...,\ K_N)$ corresponding to the selected $\hat{\vartheta}_m$s in Eq. (28) can provide an estimate of $\mathbf{B}_N$, containing the electric angle information of NFSs. By dividing the elements of the $z+1$th row of $\mathbf{h}_m$ into the corresponding elements of the zth row $(z=1,\ ...,\ N-4)$, we can extract the estimation of the electric angle ϕ_m as

$$\hat{\phi}_m=\frac{1}{2}\angle mean\left\{\frac{h_{z+1,\,m}}{h_{z,\,m}}\ :\ z\in\{1,\ ...,\ 2M-3\}\right\},\ \ m=1,\ ...,\ K_N \tag{29}$$

where $h_{z,m}$ is the element of zth row of $\mathbf{h}_m$. With Eqs. (3), (28) and (29), we can compute the range of NFSs as

$$\hat{r}_m=\pi d^2\cos\hat{\theta}_m/\lambda\hat{\phi}_m,\quad m=1,\ ...,\ K_N \tag{30}$$

where $\hat{\theta}_m$ is the mth member of $\hat{\theta}_N$.

3.6. DOA identification for FFSs by KTA

If the FFSs are located at different angles to the NFSs, then the DOAs estimated by Eq. (19) that are not contained in the vector $\hat{\theta}_N$, can be considered as the DOAs of the FFSs; i.e., the *FF candidate vector* for the azimuth angles can be considered as

$$\hat{\theta}_{FC}=\left\{\hat{\theta}_i|\hat{\theta}_i\notin\hat{\theta}_N,\ \ i=1,\ ...,\ K\right\} \tag{31}$$

where $\hat{\theta}_{FC}\in\mathbb{R}^{1\times K_F}$. However, if the FFS and NFS are located at the same angle, then there will not be a repeated DOA in Eq. (19), and an incorrect value will be declared instead. Because the presence of sources at the same angle reduces rank of $\mathbf{E}$ and, consequently, rank of $\mathbf{C}_5$. Therefore, the initial DOAs given in $\hat{\theta}$ are not necessarily correct. To solve this problem, here we present a method called the kurtosis testing algorithm (KTA) that can identify repeated DOAs and, accordingly, replace validated DOAs with incorrect initial DOAs. The KTA does not require additional data.

Given the estimated electric angles in Eq. (29) and the structure of $\mathbf{B}$ in Eq. (13), $\hat{\mathbf{B}}$ can easily be estimated. We estimate the kurtosis of NFSs from the following equation (for more details, refer to Appendix A):

$$\hat{c}_i^b=1/\left(\hat{\mathbf{b}}_i^H\mathbf{C}_1^{\dagger}\hat{\mathbf{b}}_i\right),\ \ i\in[1,\ K_N] \tag{32}$$

where $\hat{\mathbf{b}}_i$ is the ith column of $\hat{\mathbf{B}}$. Also, with the DOAs estimated by Eq. (19) and the structure of $\mathbf{E}$ in Eq. (14), $\hat{\mathbf{E}}$ can be achieved. It is

Table 1
Maximum number of resolvable sources using an ULA with N sensors for various methods.

TSMUSIC	OPMISIC	TSMDA	Ref. [3]	HODA
$K \le N-1$	$K \le (N-1)/2$	$K \le N-1$ For $K_N \le (N-1)/2$	$K \le N$	$K \le N-1$ For $K_N \le N-2$

proved that, for sources at non-repeated and repeated angles, the estimated kurtosis follow Eqs. (33) and (34), respectively (refer to Appendix A)

$$\hat{c}_i^e = 1/\left(\hat{\mathbf{e}}_i^H \mathbf{C}_5^\dagger \hat{\mathbf{e}}_i\right), \quad i \in [1,\ K] \quad \textit{For unique angles} \tag{33}$$

$$1/\left(\hat{\mathbf{e}}_i^H \mathbf{C}_5^\dagger \hat{\mathbf{e}}_i\right) = 4/\left(1/\hat{c}_i^e + 1/\hat{c}_{i'}^e\right), \quad i \in [1,\ K_N], \quad i' \in [K_N+1,\ K] \quad \textit{For } i-\textit{th source located at angle of } i'-\textit{th source}. \tag{34}$$

In Eqs. (33) and (34), $\hat{\mathbf{e}}_i$ is the ith column of $\hat{\mathbf{E}}$.

If the peer to peer NF kurtosis in Eqs. (32) and (33) were obtained identical, then we can conclude that there are no sources at repeated angles, and the FF candidate vector in Eq. (31) gives the correct DOAs for the FFSs. If the ith kurtosis of NF computed by Eq. (33) is in contradiction with the corresponding kurtosis in Eq. (32) (this means that the value of $\hat{c}_i^e$ is incorrect), then the ith DOA corresponding one should be considered as a repeated angle and eliminated one of the angles of the FF candidate vector in Eq. (31) and replaced it. To do this, we first find the kurtosis of the i'th source, which is located at the same angle as the ith source. According to Eq. (34), we have

$$\hat{c}_{i'}^b = 1/\left(4\left(\hat{\mathbf{e}}_i^H \mathbf{C}_5^\dagger \hat{\mathbf{e}}_i\right) - 1/\hat{c}_i^b\right). \tag{35}$$

Now, we replace $\hat{c}_{i'}^b$ with $\hat{c}_{i'}^e$ in Eq. (36) so that it is minimized (see Appendix B)

$$\min_{i'} \left| \frac{1}{grandsum\left(\mathbf{C}_1^\dagger\right)} - \frac{K_F^2}{1/\hat{\mathbf{c}}_{K_N+1}^e + \cdots + 1/\hat{c}_{i'}^e + \cdots + 1/\hat{c}_K^e} \right| \tag{36}$$

which $grandsum(\mathbf{C}_1^\dagger)$ represents the sum of all the values in $\mathbf{C}_1^\dagger$. In this way, we must eliminate the i'th element of $\hat{\theta}$, and replace it with ith element of $\hat{\theta}$.

3.7. Description of the proposed algorithm (HODA)

The proposed algorithm can be described as follows:

Step 1: Estimate the frequency of the signals having L snapshots by extracting the pseudospectrum using the MUSIC approach [10,11].
Step 2: Determine the appropriate number of snapshots from Eq. (15).
Step 3: Estimate $\mathbf{C}_1$, $\mathbf{C}_2$, $\mathbf{C}_3$, $\mathbf{C}_4$ and $\mathbf{C}_5$ based on L_p snapshots.
Step 4: Implement the singular-value decomposition (SVD) of $\mathbf{C}_5$ and form the reconstructed matrix $\breve{\mathbf{C}}_5$ from Eq. (16).
Step 5: Obtain the DOA estimation matrix $\mathbf{C}_{DOA}$ from Eq. (17).
Step 6: Implement the EVD of $\mathbf{C}_{DOA}$ and obtain the IDOAS.
Step 7: Obtain DCMs $\mathbf{C}_{21}$ and $\mathbf{C}_{43}$ from Eq. (22).
Step 8: Form the NF estimation matrix $\mathbf{C}_N$ and obtain the reconstructed matrix $\breve{\mathbf{C}}_N$.
Step 9: Implement the EVD of $\breve{\mathbf{C}}_N$, and obtain the NFSs' azimuth angles vector given Eqs. (27) and (28).
Step 10: Estimate the electric angles ϕ_m from Eq. (29) where $m = 1,\ ...,\ K_N$.
Step 11: Compute the range of NFSs from Eq. (30).
Step 12: Identify FFSs by KTA described in Section 3.6.

4. Discussions

4.1. Maximum number of resolvable sources

According to the explanations given in Sections 3.3 and 3.5 about $\mathbf{E}_1$ and $\mathbf{B}_N$, it is necessary the number of sensors with the ULA configuration satisfies both conditions $N \ge K_N + 2$ and $N \ge K + 1$. Therefore, in HODA, the maximum number of resolvable sources with N sensors is equal to $N-1$. On the other hand, considering Eq. (29), it is obvious that for the estimation of ϕ_m, $\mathbf{h}_m$ must have at least two rows (i.e. $N-4 \ge 1$). This means that HODA requires at least five sensors. The maximum number of resolvable sources in the various methods is summarized in Table 1. As it is evident, HOSTA has better performance than OPMUSIC in terms of avoiding aperture loss and is comparable with TSMUSIC and TSMDA. However, TSMUSIC having less than seven sensors cannot be able to estimate the range, because the vector $\mathbf{g}$ (see Eq. (33) in [1]) should at least comprise of two members. Also in TSMDA, the maximum number of NFSs which can be estimated is less than half of the number of sensors [13]. Whereas this restriction is only equal to the number of sensors minus two for HODA.

4.2. Estimation accuracy

Based on the FOC algorithm, the kurtosis of Gaussian noise is equal to zero. Whereas in SOS-based methods, noise power appears in the covariance matrix. Therefore, in FOC-based methods, the estimation accuracy will increase as the noise effect decreases. On the other hand, by selecting the proper number of snapshots in the proposed algorithm, the differencing errors decrease. Therefore, by reducing both the noise effect and the differencing errors, it is expected that the estimation accuracy in HODA will be better than OPMUSIC and TSMDA.

4.3. Computational complexity

The computational complexity of HODA is compared with other methods, considering the major multiplications involved in statistical matrices construction, eigen-decomposition, and spectral search. In HODA, one covariance matrix and one FOC with dimension $N \times N$, and also four FOCs with dimension $(N-2) \times (N-2)$ are constructed from the received data. EVD is applied to one covariance matrix with dimension $N \times N$, and also to $\mathbf{C}_{DOA}$

Table 2
Computational complexity in various methods.

	Statistics Matrix Construction	Eigen Decomposition	Spectral Search
TSMUSIC	$9(N^2+(2N-1)^2)L$	$\frac{4}{3}(N^3+(2N-1)^3+K(4N+1)^3)$	$\frac{180N^2}{\Delta_\theta}$
OPMISIC	$(N^2+\frac{(N+3)^2}{4})L$	$\frac{4}{3}(N^3+\frac{(N+3)^3}{8})$	$\frac{180}{\Delta_\theta}(N^2+(\frac{N+3}{2})^2)+KN^2\frac{2D^2/\lambda-0.62\sqrt{D^3/\lambda}}{\Delta_r}$
TSMDA	N^2L	$4N^3$	$\frac{180}{\Delta_\theta}(N-1)^2+N^2(\frac{180}{\Delta_\theta}+K_N\frac{2D^2/\lambda-0.62\sqrt{D^3/\lambda}}{\Delta_r})$
Ref. [3]	$(9P+1)N^2L$	$\frac{4}{3}(N^3+P^3)$	$N^2(\frac{180}{\Delta_\theta}+K\frac{2D^2/\lambda-0.62\sqrt{D^3/\lambda}}{\Delta_r})$
HODA	$N^2L+9(N^2+4(N-2)^2)L_P$	$4(N^3+(N-2)^3)$	$\frac{N^2}{\Delta_f}$

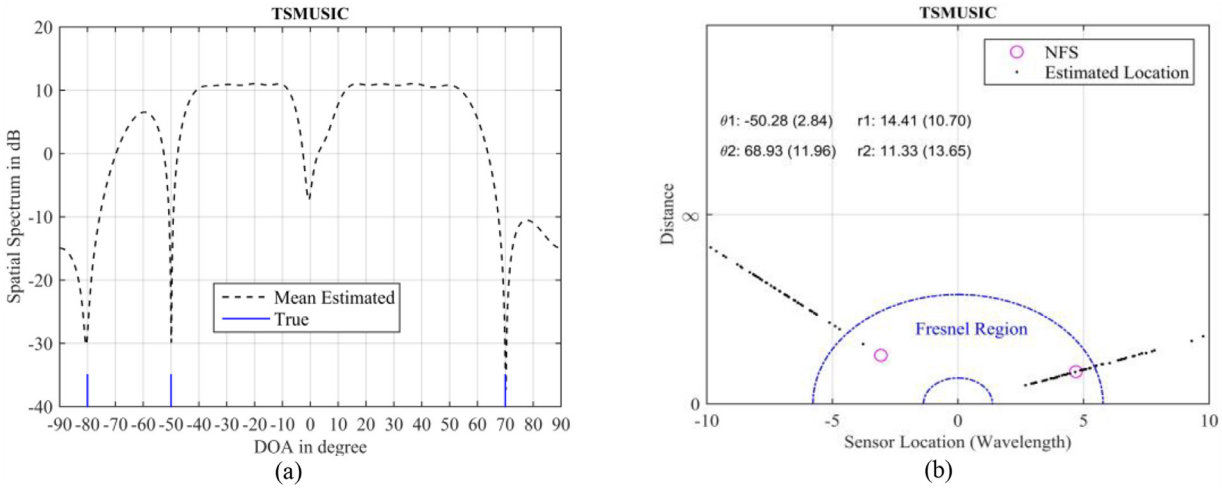

Fig. 1. Results of extracted from TSMUSIC when facing the repeated angles; (a) spatial spectrum, (b) localization of NFSs.

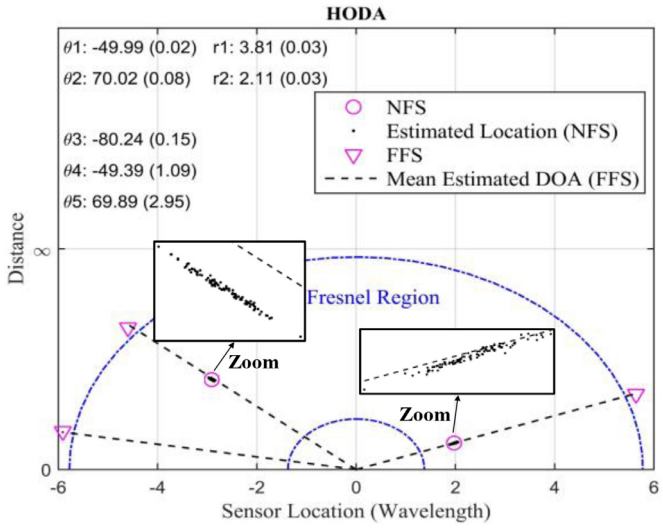

Fig. 2. Sources localization by HODA when facing the repeated angles.

and $\breve{\mathbf{C}}_N$. SVD is applied to $\mathbf{C}_5$, $\mathbf{C}_{21}$ and $\mathbf{C}_{43}$. It requires one-dimensional MUSIC spectral search, in order to estimate the frequencies. Therefore, the required number of operations in HODA is around $N^2L + 9N^2L_P + 36(N-2)^2L_P + 4N^3 + 4(N-2)^3 + \frac{N^2}{\Delta_f}$ where Δ_f is the search step for frequency in Hz. An appropriate Δ_f can be considered roughly equal to f_s/L. The computational complexities for various methods are summarized in Table 2. Δ_θ and Δ_r are the search step for angle and range in degree and wavelength, respectively. P is the number of time lags. In terms of statistics matrix construction, TSMDA and OPMUSIC have the least complexity, because they only use SOS; and the method of [3] has the most one because it requires many spatial-temporal statistical matrices. In terms of eigen-decomposition, OPMUSIC and TSMDA also have the lowest burden, and TSMUSIC has the highest computations. In terms of spectral search, HODA has the least complexity, and the other methods require a considerable volume of processing (especially for small search steps). Note that HODA with the above computational complexity, in addition to estimating the DOA and range, declares the frequency of the sources as well.

4.4. Classification of the signals types

OPMUSIC does not provide a reliable classification, because the noise components are not completely separated from the NF components. TSMDA provides a reasonable classification, with the assumption that the number of NFSs is known or correctly estimated. In HODA, by comparing the estimated DOAs derived from the differencing, and the IDOAS, number of NFSs will be known. Then, the valid FFSs are labeled according to KTA. The signals classification in HODA, unlike TSMDA, does not need to know the number of NFSs. On the other hand, due to the reduction of differencing errors, it is expected that HODA will provide a reasonable classification.

4.5. Performance limitations in specific scenarios

When NFSs and FFSs have the same angles, none of the methods of TSMUSIC and [3] is able to provide a correct estimation and classification; because the virtual steering vectors in them are solely dependent on the DOAs. Therefore, the virtual steering matrix suffers from rank loss. According to [5,14], OPMUSIC declares the spurious peaks in the estimation of FFSs. Thus it provides an unreliable estimation and classification. TSMDA distinguishes the same angles in such cases. However, it requires knowing the number of NFSs. Furthermore, TSMDA fails when two NFSs are located at 90 and −90 degrees [5]. By using KTA, HODA is able to well distinguish the sources of different fields which have the same angles.

4.6. Parameters pairing

Since both the DOA and the range of NFSs are estimated based on eigenvalues and eigenvectors of $\breve{\mathbf{C}}_N$ in parallel, HODA needs no extra operation for pairing, and such process is conducted automatically.

4.7. NF approximation model

When the source is located at the NF region, the received signal is a non-linear function of the DOA, which results in the complexity of the localization. The Fresnel approximation [15] is the most widely used method for dealing with this disadvantage. However, the use of such an approximation can reduce the accuracy of the results in practice. Since, in the case of mixed sources, the estimation accuracy of NF and FF parameters are not usually independent of each other, so the error of the NF approximation model is also effective on the estimation accuracy of the DOAs of the FFSs. Confronting this error is not the subject of this paper and can be considered as future work.

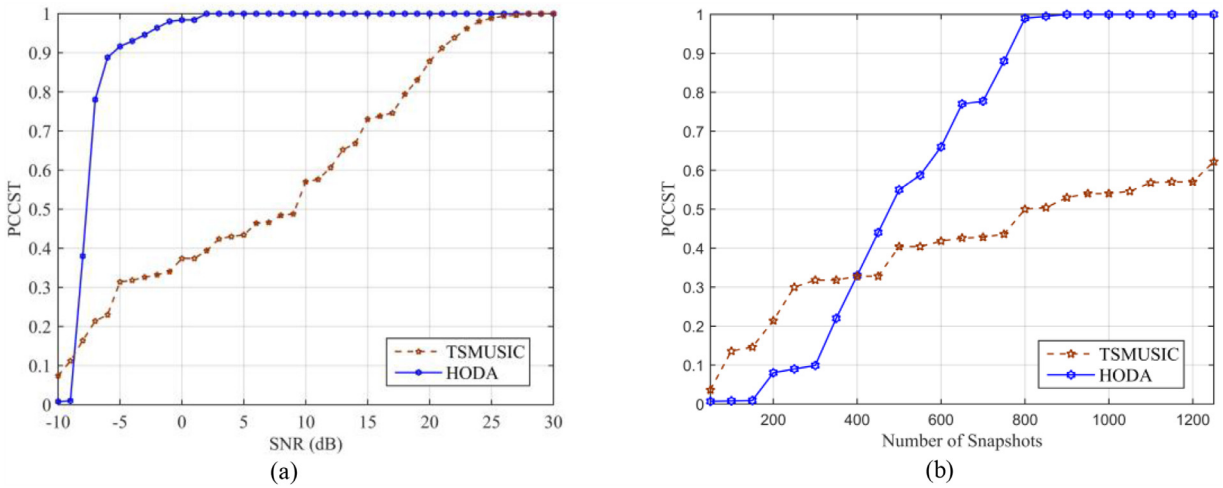

Fig. 3. Comparison of the PCCST for TSMUSIC and HODA; (a) versus SNR (L= 1000), (b) versus number of snapshots (SNR = 5dB).

4.8. Ability to localize coherent sources

In multipath environments, received signals may be uncorrelated or coherent. However, all methods reviewed in Section 1 and HODA as well, are presented for uncorrelated sources. Without assuming that the sources are uncorrelated, the elements of covariance and cumulant matrices in these methods will change and can invalidate the results; because it is a hypothesis that eliminates correlated terms and simplifies equations. Moreover, the cumulant matrices constructed in these works make use of all four indices. Therefore, they are not applicable to dealing with multipath propagation.

5. Simulation results

In this section, we present and discuss some simulations to examine the performance of the proposed algorithm. For all examples, an 11-elements ULA with element spacing 0.25λ is considered. All the impinging signals are equi-power, statistically independent, and with non-Gaussian form $s_i(t) = e^{j\omega_i t}$. The additive noise is assumed to be white complex Gaussian random process. The search steps are considered as $\Delta_\theta = 0.01^\circ$, $\Delta_r = 0.05\lambda$, $\Delta_f = 0.0001Hz$. Simulations are carried out by the approximate model (Eq. (2)), except the first part of Example 5. The estimation accuracy of HODA has been compared with TSMDA, TSMUSIC and the related Cramer–Rao bound (CRB). Since the proposed algorithm and simulations are based on the approximate NF model, the comparisons are performed based on an approximate CRB [2]. However, in the fifth example, the exact CRB of NF [7] is also considered. The results are evaluated by the root mean square error (RMSE) from the average results of many independent Monte-Carlo realizations. Also, the proposed method will be examined in terms of the probability of correct classification of signal types (PCCST) versus SNR and snapshot number. PCCST is defined as the ratio of the number of successful classification to the total number of Monte-Carlo runs. If in a run, the field type of all sources is correctly estimated, then this means the correct classification in that run.

Example 1. In the first experiment, we examine the performance of the proposed method in facing the problem of the presence of NF angles repeated in FF. We will also show that TSMUSIC and similar methods (like the method of [3]), will fail in such scenarios. Here two NFSs and three FFSs are located in $(\theta_1 = -50^\circ, r_1 = 3.8\lambda)$, $(\theta_2 = 70^\circ, r_2 = 2.1\lambda)$, $(\theta_3 = -80^\circ, r_3 = \infty)$, $(\theta_4 = -50^\circ, r_4 = \infty)$ and $(\theta_5 = 70^\circ, r_5 = \infty)$, respectively. The SNR is 15 dB and the number of snapshots L is 1000. Fig. 1(a) shows the spatial spectrum obtained by averaging 100 independent trials in TSMUSIC. As can be seen, in addition to the valleys created at approximately −80, −50 and 70 degrees, a spurious valley is also created at approximately 0°, whereas there is no source there. The location estimation of NFSs by TSMUSIC for 100 independent trials is observed in Fig. 1(b). As can be seen, the mechanism presented in TSMUSIC fails to correctly estimate the location of the NFSs. This is due to the fact that spatial spectrum in TSMUSIC is generated on the basis of a matrix in which its virtual steering vectors are only dependent on angle. Therefore, the rank loss occurs naturally for the virtual steering matrix when facing the repeated angles. The method [3] also has exactly the similar problem. Fig. 2 shows the sources localization by HODA for 100 independent trials. As can be seen, although two NFSs have the same DOAs as two FFSs, HODA has been able to detect all five sources and classify them in the correct field type. Employing KTA to eliminate invalid DOAs and identify the correct FFSs is the success reason of HODA in such a scenario.

Example 2. In the second experiment, the PCCST in HODA has been compared with TSMUSIC versus SNR and snapshot number in 500 Monte-Carlo runs. Here two NFSs and one FFS are located at $(\theta_1 = -7^\circ, r_1 = 2.2\lambda)$, $(\theta_2 = 51^\circ, r_2 = 4\lambda)$ and $(\theta_3 = -7^\circ, r_3 = \infty)$, respectively. Fig. 3(a) shows the comparison of the PCCST versus SNR for TSMUSIC and HODA. The snapshot number L is set equal to 1000. As can be seen, the PCCST is equal to 1 for SNRs above 1 dB in HODA, whereas this probability is realized in the TSMUSIC for SNRs above 27 dB. Fig. 3(b) shows the comparison of the PCCST versus the number of snapshots for TSMUSIC and HODA. The SNR is set equal to 5 dB. As can be seen, the PCCST is equal to 1 for snapshot numbers above 850 in HODA. Whereas in the TSMUSIC, the PCCST is reached 0.5 and 0.62 for the snapshot numbers 850 and 1250, respectively. The reason for the superiority of HODA is the effect of the KTA in the proposed algorithm. Basically, the TSMUSIC is based on the assumption of inequality at DOAs of all sources, and it has no solution for repeated angles. As it was noted in Section 4.4, for classification, TSMDA requires knowing the number of NFSs. Whereas HODA has no need for knowing the number of NFSs or FFSs.

Example 3. In the third experiment, we examine the estimation accuracy of HODA versus SNR and snapshot number. Here it is assumed that two NFSs and two FFSs are located at $(\theta_1 = 20^\circ, r_1 = 1.6\lambda)$, $(\theta_2 = 40^\circ, r_2 = 2.9\lambda)$, $(\theta_3 = 0^\circ, r_3 = \infty)$ and $(\theta_4 = -40^\circ, r_4 = \infty)$, respectively. In the first stage, the snapshot

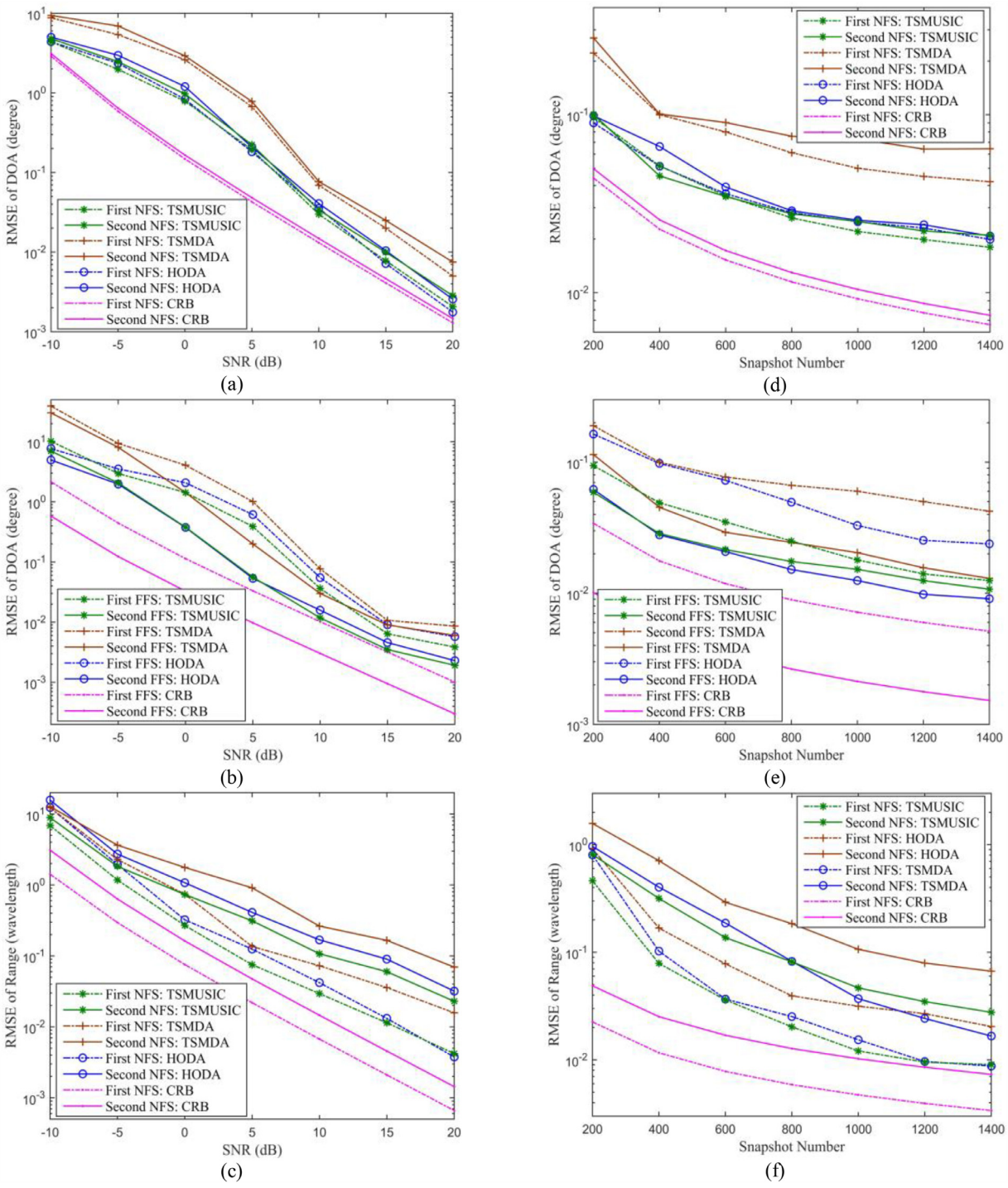

Fig. 4. RMSE of DOA and range estimations for two NFSs and two FFSs; right and left figures visualize RMSE versus the SNR and snapshot number, respectively.

number L is fixed at 700, and the SNR varies from −10 to 20 dB. In each SNR, 500 independent Monte-Carlo tests are performed. The RMSE of DOA and range estimations for HODA are displayed in Fig. 4(a)–(c), and compared with TSMDA (which also is based on statistical differencing), TSMUSIC (which also is based on some special cumulant matrices) and the related CRB. In the second stage, the SNR is fixed at 10 dB. When snapshot number varies from 200 to 1400, the RMSEs of DOA and range estimations for HODA are displayed in Fig. 4(d)–(f), and compared with TSMDA, TSMUSIC, and the related CRB. At each snapshot number, 500 independent Monte-Carlo simulations are realized. From Fig. 4, we can see that HODA has better performance than TSMDA, and the estimated diagrams are closer to the related CRB, in terms of both DOAs (for both NFSs and FFSs) and range estimations. It is also competitive with TSMUSIC. Note that in the range estimation, the first source, which is closer to the array has a smaller RMSE than that of the second source whereas the RMSEs of DOA estimations are approximately similar for both sources. This is compatible with the theoretical analyses in reference [9]. The Methods of based on HOS require a larger number of snapshots [16], and Fig. 4(a)–(c) confirms it. We can see that the estimation accuracy superiority of HODA (which is based on FOCs) compared to TSMDA (which is based on

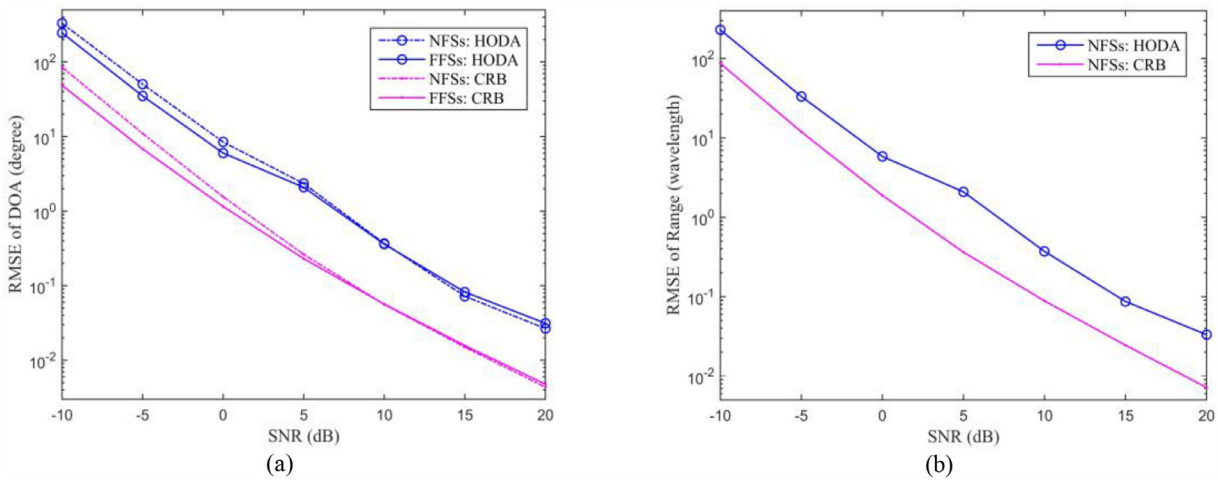

Fig. 5. Total RMSE for random parameters (number of sources, DOA and range) using HODA versus SNR (L= 700); (a) RMSE of DOAs, (b) RMSE of range.

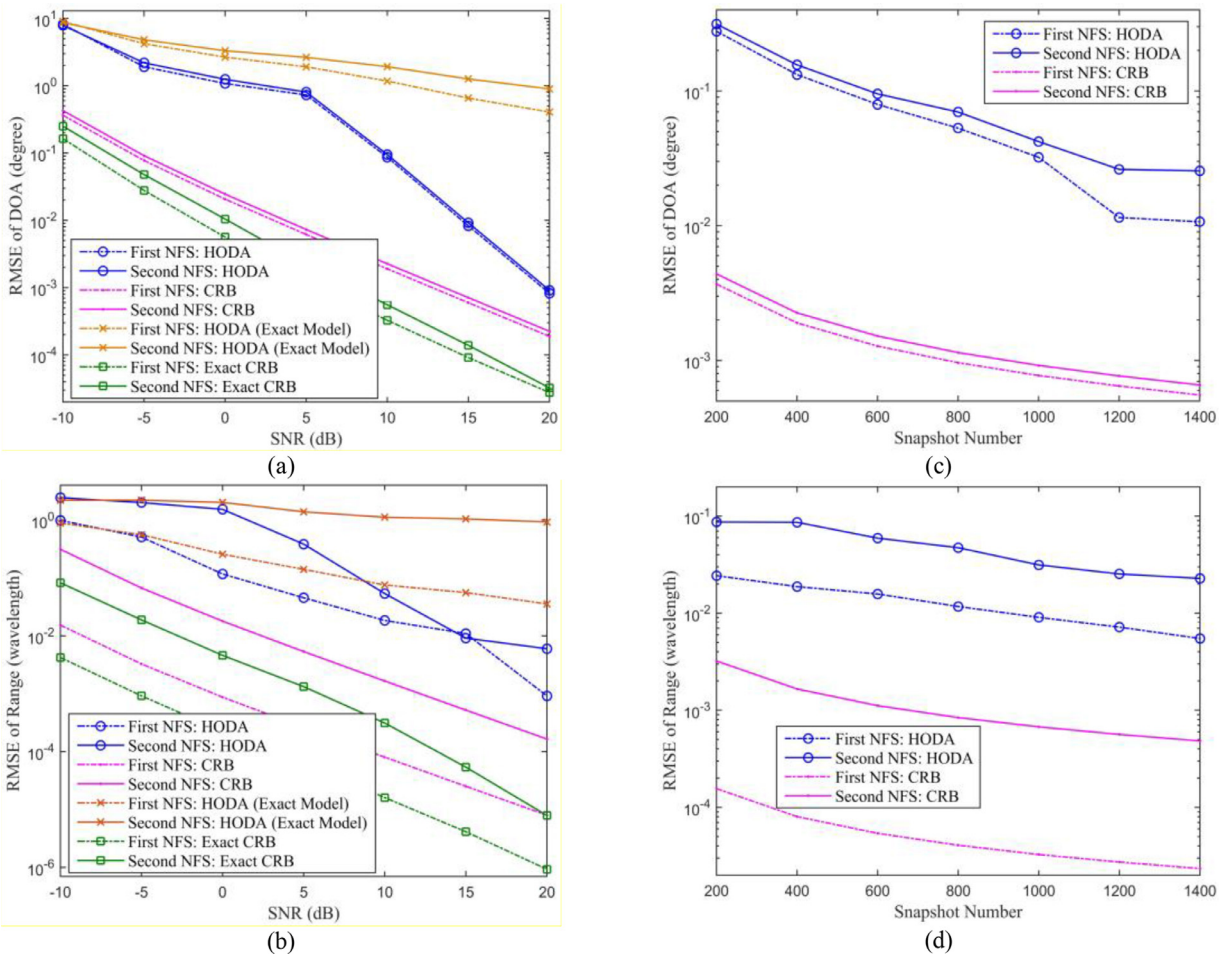

Fig. 6. RMSE of DOA and range estimations for two pure NFSs using HODA; right and left figures visualize RMSE versus the SNR and snapshot number, respectively.

SOS) is higher for a large number of snapshots than few snapshots. For example, for snapshot numbers 200 and 1400, the maximum difference percentages of RMSE of FFSs in HODA relative to CRB are equal to 428% and 759%, respectively; whereas the corresponding values in TSMDA are equal to 383% and 301%.

Example 4. In the fourth experiment, the performance of HODA is examined by random parameters. Suppose the total number of sources, their DOAs, and the ranges of NFSs are uniformly distributed in $[3, N-1]$, $[-90^\circ, 90^\circ]$ and $[1.5\lambda, 6.48\lambda]$, respectively. The number of NFSs and FFSs are chosen as $\lfloor (K-1)/2 \rfloor$ and $K - \lfloor (K-1)/2 \rfloor$, respectively. To maintain the resolution, the minimum difference between the angle of sources is considered 10°. Fig. 5 shows the total RMSE for this scenario using HODA versus SNR. In each SNR, 500 independent Monte-Carlo tests are performed. As can be seen in the random parameters scenario, the proposed algorithm is still able to execute the estimations.

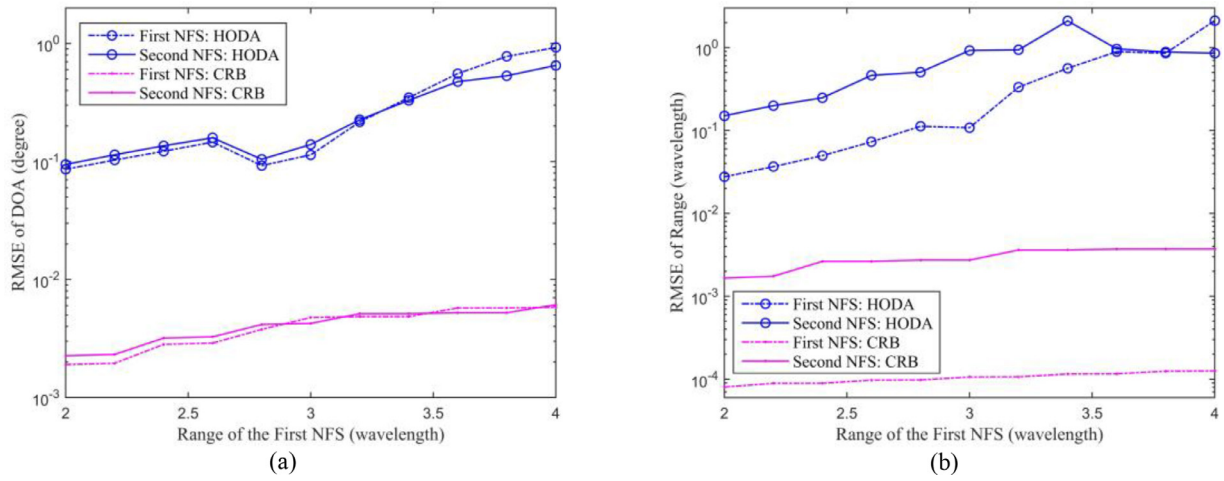

Fig. 7. RMSE of estimations for two NFSs using HODA versus varied range of the first source; (a) DOA estimations, (b) range estimations.

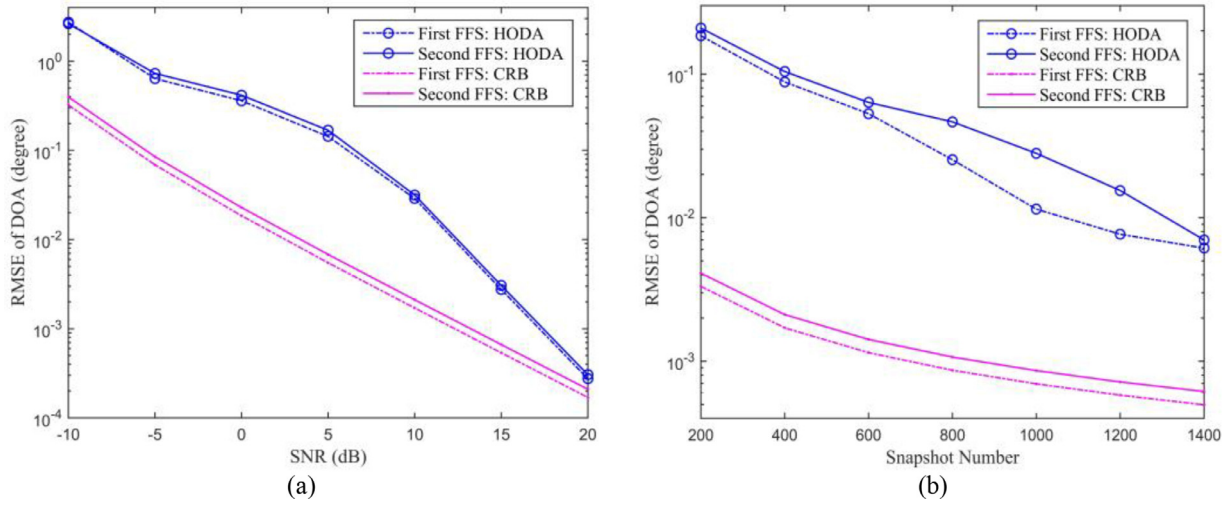

Fig. 8. The RMSE of DOA estimations for two pure FFSs using HODA; (a) versus SNR, (b) versus snapshot number.

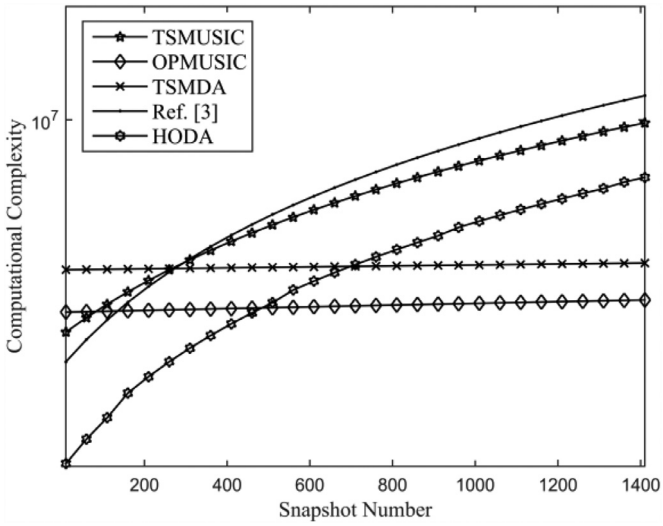

Fig. 9. Computational complexity of different methods versus the snapshot number.

Example 5. The proposed algorithm structure, theoretically, has no problem with pure sources scenario. In the fifth experiment, HODA is used to deal with pure NFSs and FFSs. In each scenario, 500 independent Monte-Carlo tests are performed.

State (1) *Pure NFSs:* Two NFSs are located at $(\theta_1 = -10^\circ, r_1 = 2\lambda)$ and $(\theta_2 = 28^\circ, r_2 = 4\lambda)$. In the first stage, the snapshot number is set equal to 400. When SNR varies from -10 to 20 dB, the RMSEs of DOA and range estimations are shown in Fig. 6(a) and (b), respectively. It can be seen that HODA has been able to estimate the parameters of both sources with acceptable accuracy for all SNRs. In addition to the approximate NF model (Eq. (2)), we also implemented the simulation based on the exact model (Eq. (1)). We also considered the exact CRB derived in [7] as a comparison. The results are shown in Fig. 6(a) and (b). As expected, the results of the parameters estimation resulting from the exact model have higher RMSE values. Because the proposed algorithm is based on an approximate model. In the second stage, the SNR is fixed at 10 dB. When snapshot number varies from 200 to 1400, the RMSEs of the DOA and range estimations are shown in Fig. 6(c) and (d). We can see that HODA still has acceptable estimation accuracy for all snapshots. In the third stage, let snapshot number and SNR be 400 and 10 dB, respectively. When the range of the first source varies from two to four wavelength, the RMSEs of the DOA and range estimations are shown in

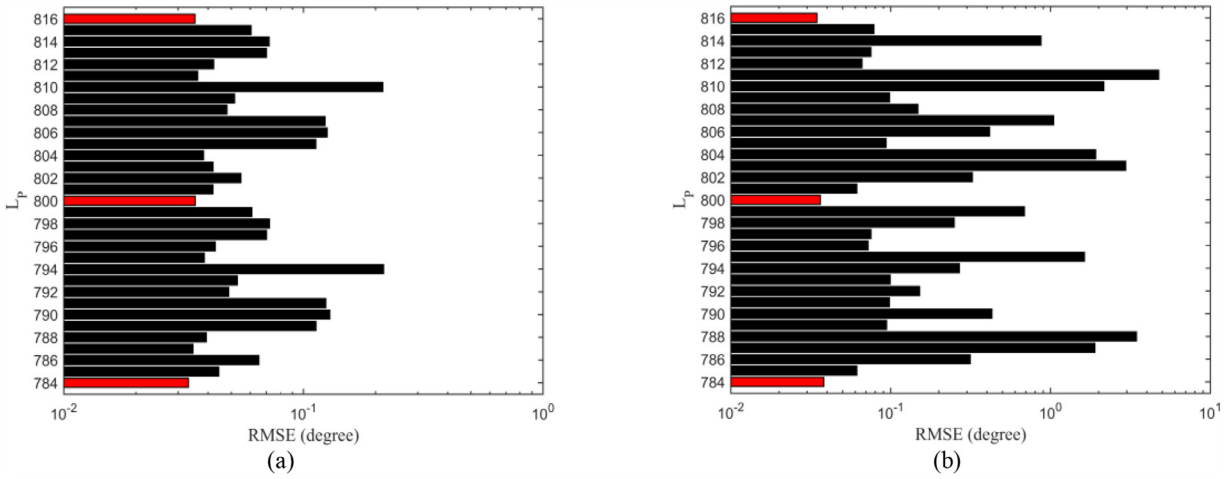

Fig. 10. RMSE of estimated angles in Example 5; (a) for $\hat{\theta}_1$, (b) for $\hat{\vartheta}_1$.

Fig. 7(a) and (b), respectively. We can see that the RMSE changes are almost consistent with CRB changes, for both DOA and range estimations. The results of all stages are in good agreement with the theoretical analyses in [9].

State (2) *Pure FFSs:* Two FFSs are located at $(\theta_1 = -10^\circ, r_1 = \infty)$ and $(\theta_2 = 28^\circ, r_2 = \infty)$. In the first stage, the snapshot number is set equal to 400. When SNR varies from −10 to 20 dB, the RMSEs of DOA estimations are shown in Fig. 8(a). In the second stage, the SNR is fixed at 10 dB. When the snapshot number varies from 200 to 1400, the RMSEs of the DOA estimations are shown in Fig. 8(b). It can be seen that HODA has been able to estimate the parameters of both sources with acceptable accuracy for all SNRs and snapshots.

Example 6. In the sixth experiment, the computational complexity of the five methods have been compared with together. The assumptions are all in line with parameters of Example 3. Fig. 9 shows the computational complexity of HODA in comparison with the other methods versus snapshot number. It can be seen that HODA has much lower complexity for small snapshots in comparison with the others. The elimination of the heavy spectral search for DOA and range estimations is the main reason for this excellence. However, considering the analysis of Section 4.3, it is clear that as the snapshot number increases, the term related to statistics matrix construction becomes the dominant term and the total complexity follows that. The dominant term in the total computational complexity of the TSMDA and OPMUSIC is the spectral search which is independent of snapshot number. Therefore, their diagram slope does not change much as the snapshot number varies. From Fig. 9, it can be seen that for $L = 700$, the computational complexity of HODA is approximately equal to TSMDA's. However, Fig. 4(a)–(c) shows that HODA, despite having a lower computational burden, has a better performance in the estimation of all parameters. Also, HODA has less computational complexity than TSMUSIC. However, its estimation accuracy is close to TSMUSIC.

Example 7. Among the estimated parameters, the value of $\hat{\vartheta}_i$ is entirely dependent on the differencing process, whereas there is no statistical differencing to obtain $\hat{\theta}_i$. In the last experiment, we show that how much is the dependency of error in $\hat{\vartheta}_i$ and $\hat{\theta}_i$ to the proper selection of the snapshot number. Here, it is assumed that one NFS and three FFSs are located at $(\theta_1 = 20^\circ, r_1 = 2.6\lambda)$, $(\theta_2 = 0^\circ, r_2 = \infty)$, $(\theta_3 = -40^\circ, r_3 = \infty)$ and $(\theta_4 = -20^\circ, r_4 = \infty)$, with frequencies of 0.5, 0.0625, 0.25 and 0.125 Hz, respectively. The SNR and f_s are 10 dB and 1 Hz, respectively. When L_p varies from 784 to 816, the RMSE of $\hat{\theta}_1$ and $\hat{\vartheta}_1$ for the proposed algorithm are displayed in Fig. 10(a) and (b), respectively. As can be seen, the RMSEs are the lowest for L_ps that are multiples of 16 (i.e. 784, 800 and 816) which are marked in a different color. This was quite expected with regard to the frequencies and the explanations in Section 3.2. Note that although the proper selection of the snapshot number has been effective on the reducing the error of both $\hat{\theta}_1$ and $\hat{\vartheta}_1$, the difference in the performance is much greater in the case of $\hat{\vartheta}_1$. Because statistical differencing greatly increases the effect of the improper selection of snapshot number on RMSE. This effect cannot be neglected for $\hat{\vartheta}_1$.

6. Conclusions

In this paper, for a symmetric ULA, a high-order differencing algorithm is presented to estimate parameters of mixed NFSs and FFSs. A mechanism based on the frequency of signals is introduced for the proper selection of snapshot number. It has been shown that the proposed mechanism can greatly reduce the errors caused by the differencing. Furthermore, to improve the estimation accuracy, a rank modification has been introduced. It was shown that HODA has good estimation accuracy in comparison with TSMDA (which also is based on statistical differencing). It was also shown that HODA is competitive with TSMUSIC (which also is based on some special cumulant matrices). In SNR 10 dB and snapshot number 700, HODA achieved the minimum RMSE of 0.01° in DOA estimation and 0.04λ in range estimation. To efficiently separate NFSs and FFSs which have the same angles, KTA is introduced. For snapshot number 1000 and SNRs above 1 dB, HODA reached PCCST=1. In small snapshot number, HODA has very low computational complexity because of the elimination of heavy computations of the spectral search. Since both DOA and range parameters are estimated based on the eigenvalues and eigenvectors belonging to one given matrix, the pairing is avoided.

In summary, the key features of HODA are: (I) for the first time, it presents a technique based on spatial differencing in the HOS domain to efficiently separate components of mixed sources; (II) it is an ESPRIT-like method and does not require any heavy spectral search to estimate DOA and range; (III) the pairing is executed automatically; (IV) it has a low aperture loss; (V) during the implementation, it also provides estimates of the frequency and kurtosis of signals.

Appendix A. The derivation of Eqs. (32)–(34)

Considering **E**, when there are no repeated angles, the kurtosis of the ith signal can be computed as

$$c_i^e = 1/\left(\varepsilon_i^H diag[1/c_1^e, \ldots, 1/c_K^e]\varepsilon_i\right), \quad i \in [1, K] \tag{A.1}$$

where $\boldsymbol{\varepsilon}_i$ is the ith column of the $K \times K$-dimensional identity matrix. Due to the fact that $\mathbf{E}^{\dagger}\mathbf{e}_i = \varepsilon_i$, we have

$$c_i^e = 1/\left(\mathbf{e}_i^H \mathbf{E}^{\dagger^H} \mathbf{C}_s \mathbf{E}^{\dagger} \mathbf{e}_i\right), \quad i \in [1, K]. \tag{A.2}$$

According to the property of $\mathbf{E}^{\dagger^H} = \mathbf{E}^{H\dagger}$, we further obtain Eq. (33). But, when ith NFS is located at the angle of i'th FFS, the ith and i'th rows of $\boldsymbol{\varepsilon}_i$ are equal to 0.5, and the rest of them are zero, where $i \in [1, K_N]$ and $i' \in [K_N + 1, K]$. So, in this case, we have

$$\varepsilon_i^H diag[1/c_1^e, \ldots, 1/c_K^e]\varepsilon_i = 1/\left(0.5^2 c_i^e\right) + 1/\left(0.5^2 c_{i'}^e\right) \tag{A.3}$$

which Eq. (34) is obtained. Similarly Eq. (32) is derived.

Appendix B. The derivation of Eq. (36)

It can be shown that in the case of FFSs, we have

$$\varepsilon_{i'} = [\mathbf{0}_{K_N \times 1} \quad (1/K_F)\mathbf{J}_{K_F \times 1}]^T, \quad i' \in [K_N + 1, K]. \tag{B.1}$$

Therefore,

$$\begin{aligned} \varepsilon_{i'}^H diag[1/c_1^e, \ldots, 1/c_K^e]\varepsilon_{i'} &= 1/\left(K_F^2 c_{K_N+1}^e\right) + \cdots + 1/\left(K_F^2 c_K^e\right) \\ &= \left(1/\hat{c}_{K_N+1}^e + \cdots + 1/\hat{c}_K^e\right)/K_F^2 \end{aligned} \tag{B.2}$$

that is $1/c_{i'}^e$. Notice that for FFSs, $\mathbf{b}_{i'}^H \mathbf{C}_1^{\dagger} \mathbf{b}_{i'} = grandsum(\mathbf{C}_1^{\dagger})$, because $\mathbf{b}_{i'} = \mathbf{J}_{(N-2)\times 1}$.

References

[1] J. Liang, D. Liu, Passive localization of mixed near-field and far-field sources using two-stage music algorithm, IEEE Trans. Sig. Process. 58 (2010) 108–120.
[2] J. He, M. Swamy, M.O. Ahmad, Efficient application of MUSIC algorithm under the coexistence of far-field and near-field sources, IEEE Trans. Sig. Process. 60 (2012) 2066–2070.
[3] J. Xie, H. Tao, X. Rao, J. Su, Passive localization of mixed far-field and near–field sources without estimating the number of sources, Sensors 15 (2015) 3834–3853.
[4] G. Liu, X. Sun, Spatial differencing method for mixed far-field and near-field sources localization, IEEE Sig. Process. Lett. 21 (2014) 1331–1335.
[5] G. Liu, X. Sun, Two-stage matrix differencing algorithm for mixed far-field and near-field sources classification and localization, IEEE Sens. J. 14 (2014) 1957–1965.
[6] J. Liang, Joint azimuth and elevation direction finding using cumulant, IEEE Sens. J. 9 (2009) 390–398.
[7] Y. Begriche, M. Thameri, K. Abed-Meraim, Exact conditional and unconditional Cramér–Rao bounds for near field localization, Digit. Sig. Process. 31 (2014) 45–58.
[8] E. Grosicki, K. Abed-Meraim, Y. Hua, A weighted linear prediction method for near-field source localization, IEEE Trans. Sig. Process. 53 (2005) 3651–3660.
[9] N. Yuen, B. Friedlander, Performance analysis of higher order ESPRIT for localization of near-field sources, IEEE Trans. Sig. Process. 46 (1998) 709–719.
[10] P. Stoica, R.L. Moses, Spectral Analysis of Signals, 1, Pearson Prentice Hall, Upper Saddle River, NJ, 2005.
[11] R. Schmidt, Multiple emitter location and signal parameter estimation, IEEE Trans. Antennas Propag. 34 (1986) 276–280.
[12] R. Roy, T. Kailath, ESPRIT-estimation of signal parameters via rotational invariance techniques, IEEE Trans. Acoust. Speech Sig. Process. 37 (1989) 984–995.
[13] J. Xie, H. Tao, X. Rao, J. Su, Comments on Near-field source localization via symmetric subarrays, IEEE Sig. Process. Lett. 22 (2015) 643–644.
[14] J.-H. Lee, C.-M. Lee, K.-K. Lee, A modified path-following algorithm using a known algebraic path, IEEE Trans. Sig. Process. 47 (1999) 1407–1409.
[15] W. Zhi, M.Y.-W. Chia, Near-field source localization via symmetric subarrays, in: *Proceedings of the IEEE International Conference on Acoustics, Speech and Signal Processing (ICASSP 2007*, IEEE, 2007, pp. II–1121. II-1124.
[16] A. El Gonnouni, M. Martinez-Ramon, J.L. Rojo-Alvarez, G. Camps-Valls, A.R. Figueiras-Vidal, C.G. Christodoulou, A support vector machine music algorithm, IEEE Trans. Antennas Propag. 60 (2012) 4901–4910.